Comparison of Stator- and Rotor-Force Excitation for the Acoustic Simulation of an Induction Machine with Squirrel-Cage Rotor

C. Schlensok and G. Henneberger

Institute of Electrical Machines (IEM), RWTH Aachen University, Germany
Schinkelstraße 4, D-52056 Aachen, Germany, phone: (+49 241 8 09 76 67), fax: (+49 241 8 09 22 70)
e-mail: Christoph.Schlensok@iem.rwth-aachen.de

I. INTRODUCTION

The drivers of passenger cars nowadays make great demands on the acoustics of the technical equipment such as the electrical power steering. Therefore, it is of high interest to estimate the audible noise radiation of these components. The induction machine with squirrel cage rotor used as power-steering drive is computed in three steps:

1. electromagnetic simulation,
2. structural-dynamic computation, and
3. acoustic estimation.

The theory is briefly described in [1] and therefore not repeated.

In the case of an induction machine with skewed squirrel-cage rotor the location of the maximum force excitation of the stator teeth depends on the rotational direction. Sofar, only stator teeth excitation has been regarded in literature [2][3][4]. Further on the impact of the force exciting the rotor is taken into account. Therefore, four different cases of electromagneitc surface-force excitation are compared and discussed in this paper as listed in Table 1.

Table 1: Cases for Different Force Excitations.

type of excitation	rotational direction
stator-teeth	left-hand
rotor-teeth	right-hand
stator-teeth	right-hand
rotor- & stator-teeth	right-hand

Since the rotor of the induction machine is skewed (skewing angle $\gamma = 10°$) the stator teeth are excited very asymmetrically. The location of the maximal tooth excitation depends on the direction of rotation. In case of right-hand rotation the highest excitation values are positioned on the side of the mounting plate. Left-hand rotation results in maximal excitation locations on the opposite side of the machine. For this, both directions are computed and the audible acoustic-noise radiation is compared. Fig. 1 defines the rotational direction.

Usually it is sufficient to simply take the force excitation of the stator into consideration to make good predictions of the radiated noise. The stator of the regarded machine is weakly coupled to the casing mechanically spoken by hard rubber rings around the casing caps and steel-spring pins in the notches of the stator and casing. The rotor on the other hand is strongly coupled to the casing caps by the bearings. For this, the rotor excitation has to be taken into account as well for comparison reasons.

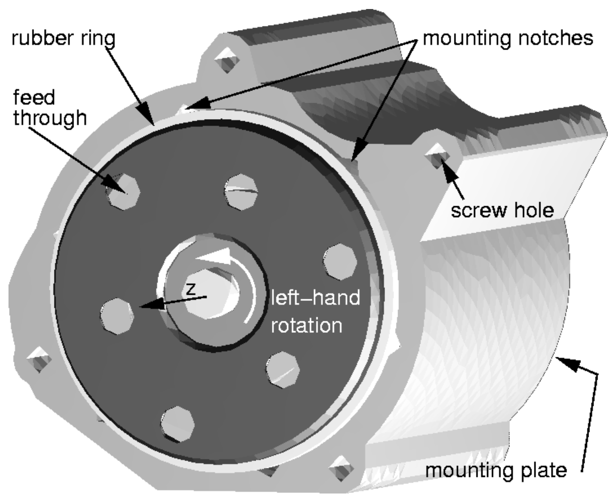

Figure 1: Definition of Rotational Direction; Location of the Mounting Plate, the Mounting Notches, the Screw Holes, and the Rubber Rings.

II. ELECTROMAGNETIC SIMULATION

The first step of the computational process is the electromagnetic simulation. The induction machine is simulated with a 3-dimensional magnetostatic model which uses stator and rotor currents as excitations. Due to computational time-saving reasons the rotor-bar currents are derived from a 2-dimensional, transient computation [5]. The 2D model constists of 6,882 first order triangular elements and the computation of one time step in 2D takes $\bar{t}_{2D} = 24.7\,\mathrm{s}$. A 3D time-step simulation takes $\bar{t}_{3D} \approx 494\,\mathrm{min}$ due to 288,782 first order tetrahedrian elements in the 3D model. The duration of the transient phenomenom t_{tp} equals the rotor-time constant t_R:

$$t_{tp} = t_R \approx 0.1\,\mathrm{s}\,. \tag{1}$$

Depending on the time step Δt ($\Delta t_{3D} = 416.\overline{6}\,\mu\mathrm{s}$) the number of time steps "lost" N_{lost} for analysis is:

$$N_{lost} = \frac{t_{tp}}{\Delta t} = 240\,. \tag{2}$$

In the case of transient 3D simulation the extra simulation time would approximately sum up to:

$$t_{extra} \approx N_{lost} \cdot \bar{t}_{3D} - N_{lost} \cdot \bar{t}_{2D} = 3,576\,\mathrm{h} = 149\,\mathrm{d}\,. \tag{3}$$

The 3D static simulation can be performed simultaneously on several computers. So that the effective computational time is reduced drastically to about 3 weeks in total, for both: the 2D transient and 3D static simulation.

Two global results are provided:

1. the net force onto the rotor and
2. the torque of the machine for each time step.

Due to the symmetry of the machine only a half model has to be applied and the radial and tangential components of the net force cannot be computed. Therefore, only the axial component of the net force and the torque are analyzed. All electromagnetic simulations are performed employing the open-source software *i*MOOSE of the IEM [6].

The studied point of operation is at nominal speed $n_N = 1200\,\mathrm{rpm}$ and $f_1 = 48.96\,\mathrm{Hz}$. $N = 120$ time steps are computed and analyzed with the 3D model. For the 2D model the equivalent time steps are taken into regard.

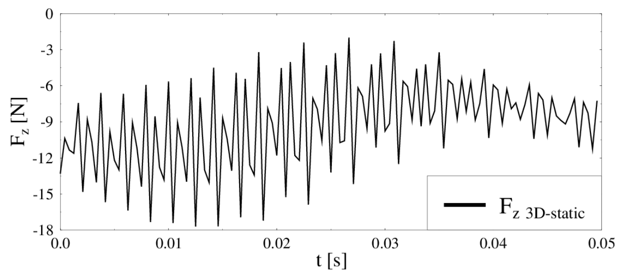

Figure 2: Net-Force Behavior for 3D Model.

The time behavior of the axial component of the net force, which depends only on the skewing angle is depicted in Fig. 2. The average value is $\overline{F}_z = 9.22\,\mathrm{N}$. The direction of the force depends on the rotational direction. In the case of left-hand rotation the force acts in negative z-direction (see Fig. 1). For right-hand rotation the rotor is dragged into the opposite direction.

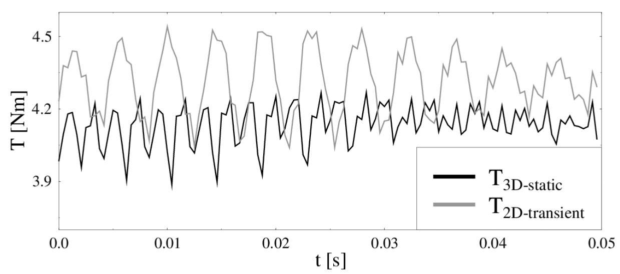

Figure 3: Torque Behavior for 2D and 3D Model.

Fig. 3 shows the time behavior of the torque for 2D transient and 3D static computation. The average value of the 3D torque is lower because of the rotor skewing and the front leakage: $\overline{M}_{3D} = 4.13\,\mathrm{Nm} < 4.31\,\mathrm{Nm} = \overline{M}_{2D}$. Both effects are neglected by the 2D model.

The net-force and the torque behavior are analyzed using the **F**ast-**F**ourier **T**ransformation (FFT) [7]. Due to the smaller time step in the case of the 2-dimensional simulation $\Delta t_{2D} = \frac{1}{3}\Delta t_{3D}$ the cut-off frequency $f_{co\,2D}$ in the spectrum is three times $f_{co,3D} = 1,200\,\mathrm{Hz}$. The time step Δt_{3D} and the number of time steps N_{3D} in case of the 3D simulation are chosen in such a way that the resolution in the frequency domain is exactly the rotor speed $f_R = 20\,\mathrm{Hz}$. The resolution of the 2D spectrum is ten times that of the 3D spectrum because of the high number of time steps $N_{2D} = 3,600$. With the Criteria of Nyquist [8] and

$$\Delta f = \frac{2 \cdot f_{co}}{N} \tag{4}$$

the resolutions of the spectra result in:

$$\Delta f_{3D} = 20\,\mathrm{Hz} \quad \text{and} \quad \Delta f_{2D} = 2\,\mathrm{Hz}\,. \tag{5}$$

Fig. 4 shows the spectrum of the axial net-force component of the 3D simulation. The main orders found are at intervals of $f_{int} = 240\,\mathrm{Hz}$. The same orders are found in the torque spectrum in Fig. 5. This reflects the very close link of the axial net-force component and the torque: The torque vector points into the axial direction. Structure-borne sound-measurements show the highest values at 720 Hz and 940 Hz next to others. These two significant orders might be caused by the axial force and torque excitation. The spectrum of the 2D simulation is similar to Fig. 5.

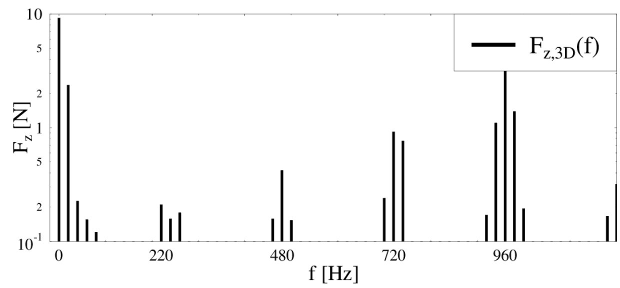

Figure 4: Spectrum of the Axial Net-Force Component of the 3D Model.

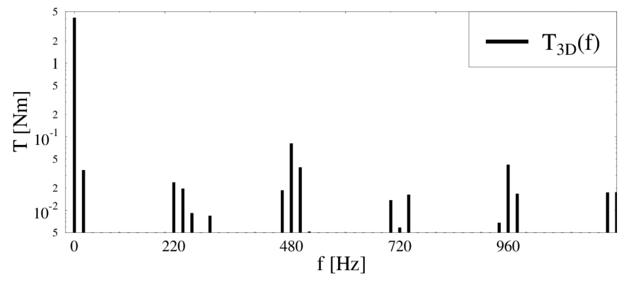

Figure 5: Spectrum of the Torque of the 3D Model.

Next to these two global values the electromagnetic computation also provides the flux-density distribution for each time step. From this the surface-force density is derived at the interface of air and the lamination of the machine [9].

Only the 3D model is regarded for the investigations in the following. For each time step the surface-force density of the stator and rotor lamination are computed of the 3D model. The excitation of each considered element is analyzed by using the FFT and transforming the forces to the frequency domain. The surface-force density-excitation for one time step is depicted in Fig. 6. The highest values are reached at the up-running edges of the stator teeth.

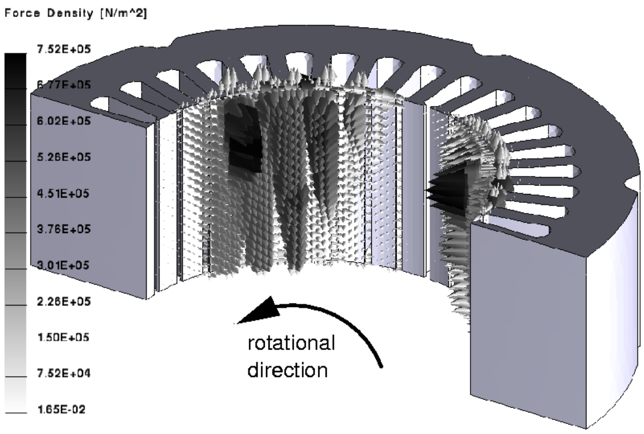

Figure 6: Surface-Force Density-Excitation for One Time Step at Left-Hand Rotation.

The surface-force excitation is transformed to the frequency domain as well. The FFT is again used. In a first step the values of the three components (x, y, and z) of all $N = 120$ time steps of each stator-surface element are collected. There are $E_{stator} = 20,602$ shell elements. Then the FFT is performed for each of these elements. Finally the transformed values for the three components are rearranged into two files (real and imaginary part) for each of the frequencies in the spectrum (number of frequencies: $N_f = 61$).

III. STRUCTURAL-DYNAMIC SIMULATION

The next step in the computational process is the simulation of the deformation of the entire machine structure due to the surface-force density-excitation derived from the electromagnetic simulation. For this, an extra model of the entire machine is generated consisting of the stator and rotor laminations including the winding and the squirrel cage, the shaft, the bearings, the casing, and the casing caps. The model is described more detailed in [1].

Four different types of force excitations are object of investigation as listed in the introductionary section of this paper. The locations of the highest force excitations depend on the rotational direction. In the case of right-hand rotation the maximal forces arise at the side of the mounting-plate of the machine (see Fig. 1 and Fig. 6). For left-hand rotation the highest excitaion is located on the opposite side.

Exemplarily, Fig. 7 shows the real and the imaginary part of the surface-force density-excitation for $f = 420\,\mathrm{Hz}$ for left-hand rotation. There is a phase shift between both parts. This will result in a pulsating deformation behavior for the excitation at this frequency. The maximal forces in both, the real and imaginary part, are positioned at four locations. The order of deformation does not depend on the rotational direction.

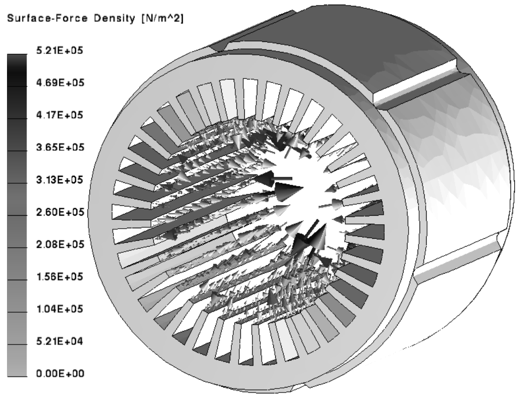

(a) Surface-Force Density-Excitation, Left-Hand Rotation, Real Part.

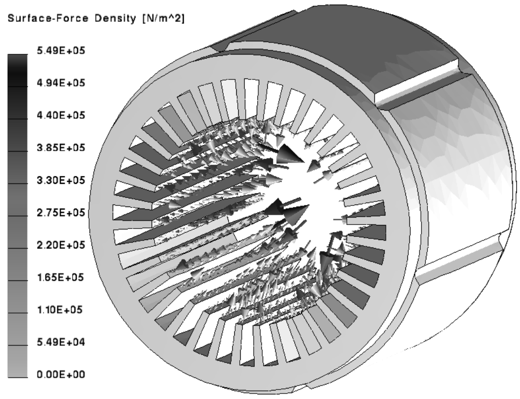

(b) Surface-Force Density-Excitation, Right-Hand Rotation, Imagnary Part.

Figure 7: Location of the Maximal Surface-Force Density-Excitation for $f = 420\,\mathrm{Hz}$ at Left-Hand Rotation: (a) Real Part, (b) Imaginary Part.

The frequencies analyzed and the resulting mechanical orders of deformation r are listed in Table 2. $r = 2$ is the most often order found. Mainly 2nd and 4th order deformations are detected. Orders higher than $r = 6$ usually do not produce strong deformation and are not critical in respect of noise radiation. The most important order is the elliptical 2nd order [10].

Table 2: Mechanical Orders of Deformation Found for all Analyzed Frequencies.

r []	f [Hz]
2	420, 520, 720, 940
4	100, 1040, 1140
6	620

The resulting deformation of the stator and the casing of the machine in the case of pure stator teeth excitation is shown in Fig. 9 in an overemphasized repre-

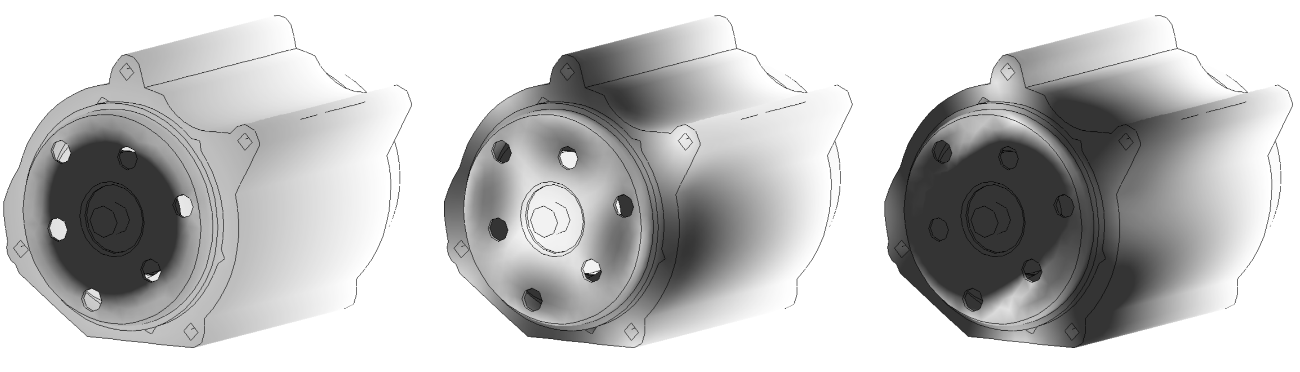

(a) Rotor-Teeth Excitation, Right-Hand Rotation, $f = 940\,\mathrm{Hz}$ (Real Part).

(b) Stator-Teeth Excitation, Right-Hand Rotation, $f = 940\,\mathrm{Hz}$ (Real Part).

(c) Rotor- and Stator-Teeth Excitation, Right-Hand Rotation, $f = 940\,\mathrm{Hz}$ (Real Part).

Figure 8: Deformation of the Entire-Machine Structure: Pure Rotor, Pure Stator, and Combined Rotor-Stator Excitation.

sentation for the frequency of $f = 620\,\mathrm{Hz}$. The spring pins keeping the stator fixed in the casing damp the deformation and decouple both parts very well. The deformation of the casing is much lower than that of the stator and cannot be sensed in the figure. Some deformation orders are shown in Fig. 10.

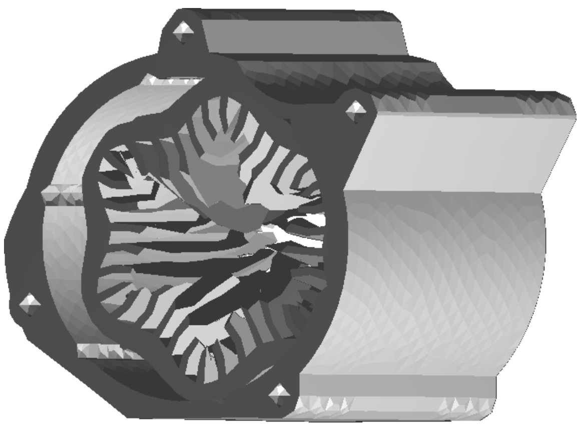

Figure 9: Deformation of the Stator at $f = 620\,\mathrm{Hz}$.

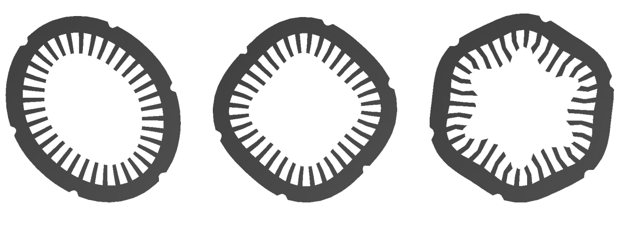

(a) $r = 2$.

(b) $r = 4$.

(c) $r = 6$.

Figure 10: Mechanical Orders of the Deformation.

Fig. 11 depicts the real part of the deformation of the entire machine structure in scalar representation at $f = 720\,\mathrm{Hz}$. Although the order of deformation of the stator deformation is $r_{stator} = 2$ the deformation order of the casing of the machine is $r_{casing} = 4$. This effect stems from the skewing and the mounting of the machine. The skewing results in torsional vibrations [5]. The machine is mounted on one front plate. This way the deformation is "reflected" at this stiff front plate and produces the double order on the opposite front plate ("open end"). In the case of right-hand rotation the maximal deformation arises on the "open end" of the structure. This is the same location of the maximal force excitation. Therefore, the deformation of the machine depends strongly on the rotational direction.

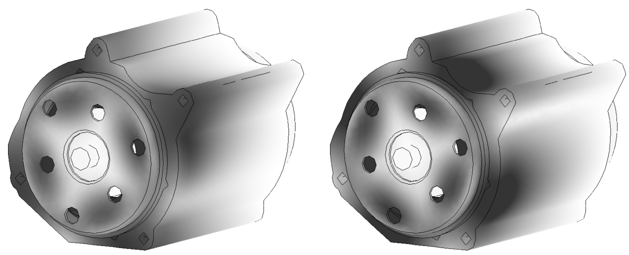

(a) Stator-Teeth Excitation, Left-Hand Rotation, $f = 720\,\mathrm{Hz}$.

(b) Stator-Teeth Excitation, Right-Hand Rotation, $f = 720\,\mathrm{Hz}$.

Figure 11: Deformation of the Entire Machine in the Case of Pure Stator-Teeth Excitation, Real Part.

In a next step the deformation stemming from the combined rotor and stator excitation at right-hand motion is simulated. Exemplarily Fig. 8 depicts the real part of the deformation for pure rotor excitation (Fig. 8(a)), pure stator excitation (Fig. 8(c)), and for combined excitation (Fig. 8(c)) at $f = 940\,\mathrm{Hz}$. All three pictures show the same scaling (black strong, white weak deformation).

Pure rotor excitation results in strong deformation of the shaft and the casing caps. This deformation mainly deforms these parts in radial and axial direction of the machine. If pure stator excitation is regarded mainly the casing at the "open end" and the outer parts of the casing caps are deformed. Finally the combination of both excitations result in strong deformation of the casing and the casing caps. These observations are stated for all studied frequencies listed in Table 2.

Next to the possibility of using the deformation of the structure for acoustic simulation the structure-borne sound at certain locations can be derived. For this reason the node nearest to the location of the accelerometer for measurements on the flank of the casing and one node on the casing cap where the converter is mounted are chosen. Fig. 12 shows the locations of the nodes regarded with their IDs. The definition of the tangential, radial, and axial direction is displayed as well.

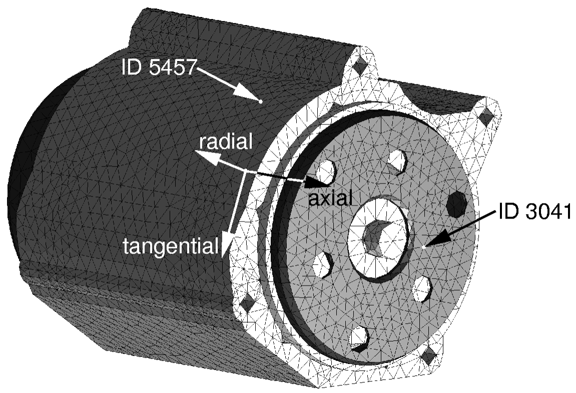

Figure 12: Locations of the Nodes for Structure-Borne Sound-Analysis.

The structure-borne sound-level L_S is calculated as follows for radial, tangential, and axial direction:

$$L_S = 20 \cdot \log \frac{a}{1\,\frac{\mu\mathrm{m}}{\mathrm{s}^2}}\,\mathrm{dB}\,. \qquad (6)$$

a is the acceleration of the specific node at the regarded frequency f [1]. Fig. 13 depicts the structure-borne sound-levels for some selected frequencies in the case of left-hand rotation and pure stator-teeth force-excitation. The axial sound level is about $\Delta L_S = 20\,\mathrm{dB}$ lower throughout the spectrum. This fact can be stated for right-hand rotation and both pure stator and combined rotor and stator excitation as well. The same levels are reached for the tangential and radial components for all regarded frequencies.

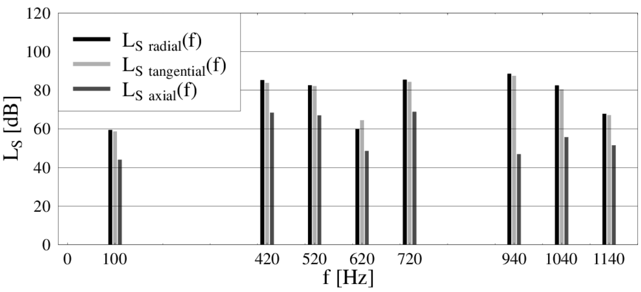

Figure 13: Structure-Borne Sound-Levels, Left-Hand Rotation, Pure Stator Excitation, ID 5457.

Referring to the deformation plot in Fig. 8(a) Fig. 14 shows exemplarily the results for the levels calculated on the casing cap (node 3041) in the case of pure rotor force-excitation for Node 3041. The three components reach nearly the same levels. The highest values are detected for $f = 620\,\mathrm{Hz}$ and $f = 720\,\mathrm{Hz}$.

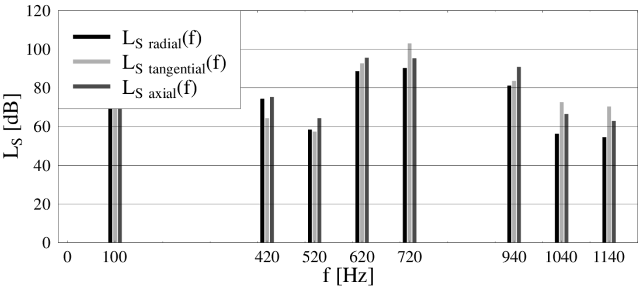

Figure 14: Structure-Borne Sound-Levels, Right-Hand Rotation, Pure Rotor Excitation, ID 3041.

Fig. 15 depicts the levels in the case of pure stator-excitation (see Fig. 8(c)) for Node 3041. Except for much lower levels at $f = 100\,\mathrm{Hz}$ and $f = 620\,\mathrm{Hz}$ slightly lower values are reached for $f = 720\,\mathrm{Hz}$. The axial component is the lowest for $f = 620\,\mathrm{Hz}$ and the higher frequencies similar to the results in Fig. 13.

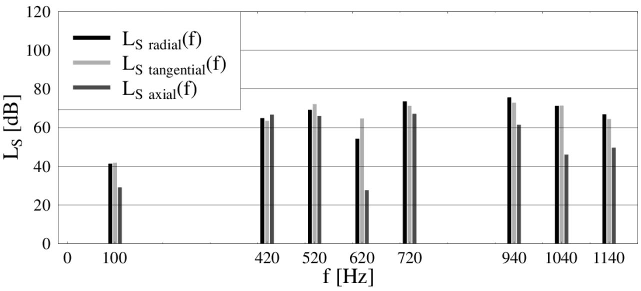

Figure 15: Structure-Borne Sound-Levels, Right-Hand Rotation, Pure Stator Excitation, ID 3041.

Finally the combined stator- and rotor-excitation is regarded. At Node 3041 the spectrum is similar to pure stator excitation with the exception of the significantly higher levels at $f = 620\,\mathrm{Hz}$ and $f = 720\,\mathrm{Hz}$. This spectrum suits the result of the acceleration measurements very well.

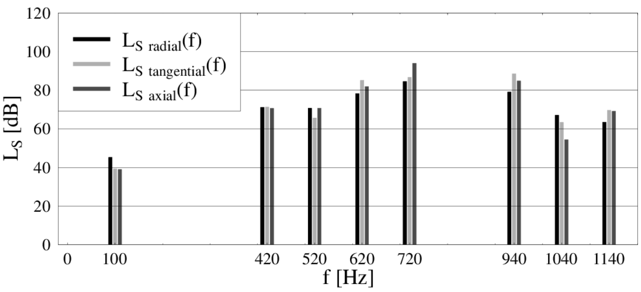

Figure 16: Structure-Borne Sound-Levels, Right-Hand Rotation, Combined Stator-Rotor Excitation, ID 3041.

It can be stated that pure stator excitation results in farely good estimations concerning the structure-borne sound-levels. Only very few orders are affected significantly by the forces acting on the rotor. These forces amplify the axial component. Therefore, it is of advantage to take the rotor excitation into account to get more exact results concering the structure-borne sound.

IV. ACOUSTIC SIMULATION

The last step is to estimate the air-borne noise generated by the different excitations. For this reason a boundary-element model of the entire machine structure is applied. The air-borne sound-pressure is estimated on an analysis hemisphere around the machine at a distance of $d = 1\,\text{m}$. Fig. 17 shows the result for stator-rotor excitation at $f = 420\,\text{Hz}$.

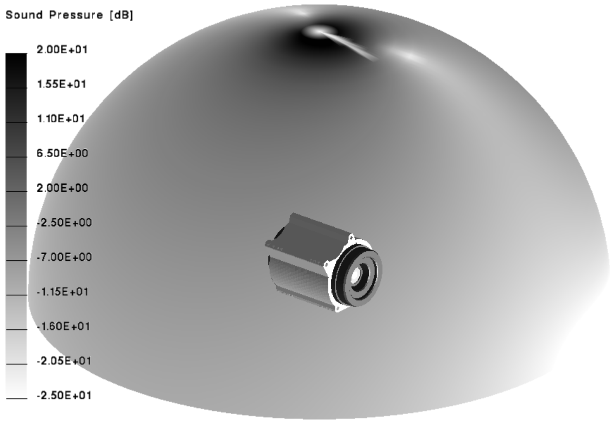

Figure 17: Sound-Pressure Distribution at $f = 420\,\text{Hz}$ for Stator-Rotor Exciation and Right-Hand Rotation.

The maximum sound-pressure levels L reached for the three cases taking the stator excitation into account are listed in Table 3.

Table 3: Maximal Levels of the Estimated Air-Borne Sound-Pressure (**sl**: **s**tator excitation, **l**eft-hand rotation; **sr**: **s**tator excitation, **r**ight-hand rotation; **srr**: **s**tator + **r**otor excitation, **r**ight-hand rotation).

f [Hz]	L_{sl} [dB]	L_{sr} [dB]	L_{srr} [dB]
420	16	26	9
520	23	23	23
620	9	6	14
720	27	25	27
940	28	29	28
1040	11	21	22
1140	9	10	10

The results show that the direction of the rotation has a significant effect on the noise generation. Except for $f = 720\,\text{Hz}$ and $f = 620\,\text{Hz}$ all orders are amplified up to $\Delta L = 10\,\text{dB}$. If the rotor-force excitation is taken into account some orders become louder and some quieter. The air-borne sound-levels do not suit the acceleration measurements as well as those of the structure-borne sound.

V. CONCLUSION

In this paper the structure- and air-borne noise of an induction machine with squirrel-cage rotor are estimated. For this, different types of surface-force excitations and rotational directions are regarded for the first time. In general the calculated structure-borne sound-levels suit the acceleration measurements of the industrial partner very well. The acoustic noise levels differ from those.

The comparison of the different excitations show, that it is necessary to take the rotor excitation into account. In case of pure stator excitation e.g. the first stator-slot harmonic at 720 Hz does not reach as significantly high levels as expected although it is one of the strongest orders measured.

VI. REFERENCES

[1] Schlensok, C., Küest, T., Henneberger, G., "Acoustic Calculation of an Induction Machine with Squirrel Cage Rotor," *16th International Conference on Electrical Machines*, ICEM, Crakow, Poland, September 2004

[2] Kim, B.-T., Kwon, B.-I., "Reduction of Electromagnetic Force Harmonics in Asynchronous Traction Motor by Adapting the Rotor Slot Number," *IEEE Transactions on Magnetics*, 35(5):3742–3744, September 1999

[3] Kobayashi, T., Tajima, F., Ito, M., Shibukawa, S., "Effects of Slot Combination on Acoustic Noise from Induction Motors," *IEEE Transactions on Magnetics*, 33(2):2101–2104, March 1997

[4] Vandevelde, L., Gyselinck, J. J. C., Bokose, F., Melkebeek, J. A. A., "Vibrations of magnetic origin of switched reluctance motors," *COMPEL*, 22(4):1009–1020, Nov 2003

[5] Arians, G., *Numerische Berechnung der elektromagnetischen Feldverteilung, der strukturdynamischen Eigenschaften und der Geräusche von Asynchronmaschinen*, Shaker Verlag, Aachen, 2001, Dissertation, Institut für Elektrische Maschinen, RWTH Aachen

[6] Arians, G., Bauer, T., Kaehler, C., Mai, W., Monzel, C., van Riesen, D., Schlensok, C., "iMOOSE," www.imoose.de

[7] Bronstein, I. N., Semendjajew, K. A., *Taschenbuch der Mathematik, 25. Auflage*, B. G. Teubner Verlagsgesellschaft, Stuttgart, Leipzig, 1991

[8] Lüke, H. D., *Signalübertragung*, Springer-Verlag, Berlin, Heidelberg, New York, 1999

[9] Ramesohl, I. H., Küppers, S., Hadrys, W., Henneberger, G., "Three Dimensional Calculation of Magnetic Forces and Displacements of a Claw-Pole Generator," *IEEE Transactions on Magnetics*, 32(3):1685–1688, May 1996

[10] Jordan, H., *Geräuscharme Elektromotoren*, Verlag W. Girardet, Essen, 1950